Seismic Tests of Precast Beam-to-Column Joint Subassemblages With Unbonded Tendons

M. J. Nigel Priestley, Ph.D.

Professor of Structural Engineering
Department of Applied Mechanics
and Engineering Sciences
University of California at San Diego
La Jolla, California

Two ungrouted post-tensioned, precast concrete beam-to-column joint subassemblages were tested under cyclic reversals of inelastic displacement to determine seismic response. One subassemblage represented an exterior joint while the other was an interior joint of a one-way prestressed concrete frame. The large scale test units were designed with greatly reduced beam and joint shear reinforcement compared with equivalent monolithic joints, but with special spiral confinement of the beam plastic hinge regions. Both subassemblages performed well, with only minor, cosmetic damage being recorded up to drift ratios of 3 percent or more. Energy absorption of the hysteretic response, though small, was larger than expected and residual displacements were negligible. It is concluded that satisfactory seismic performance can be expected from well-designed ungrouted precast, post-tensioned concrete frames.

Gregory A. MacRae, Ph.D.

Assistant Professor
Department of Civil Engineering
University of Washington
Seattle, Washington

An earlier paper[1] explored the theoretical seismic response of precast, prestressed concrete frames with partially unbonded tendons. This was done by means of dynamic inelastic time history analyses of several single degree of freedom oscillators of different periods and different hysteretic force-displacement characteristics, including bilinear elastic response. This hysteretic characteristic was shown to be representative of the response of precast systems with unbonded, or partially debonded tendons.

Results of the theoretical analyses indicated that, despite the total lack of hysteretic energy absorption in the bilinear elastic model, displacements for medium to long period structures with such a force-displacement response would be less than 35 percent larger than elasto-plastic systems of the same period. It was pointed out earlier[1] that the actual seismic responses of equivalent reinforced concrete and unbonded prestressing systems should, in fact, have very similar peak displacements. This is because reinforced concrete

plastic hinges exhibit less efficient loops than elasto-plastic systems and, hence, shorter periods than reinforced concrete frames with similar dimensions and strengths.

The disadvantages of possibly increased maximum displacement response were felt to be offset by the lack of residual displacement with the prestressed system, which is a consequence of the bilinear elastic response. The prestressed system should also show greatly reduced sensitivity to cyclic incremental increases in displacement ("crawling") resulting from P-Δ effects, compared with elasto-plastic systems. Structures with unbonded prestressed tendons could also be expected to retain a high stiffness at low displacements after responding to a major seismic event. This should help to reduce secondary damage to non-structural elements in aftershocks or future earthquakes.

Parallel design studies[1] indicated that there would be significant detailing advantages in the use of unbonded post-tensioned precast frames. These included:

- Dependable concrete shear-resisting capacity in beam plastic hinges, resulting in reduced requirements for transverse reinforcement in beams.
- Joint shear transferred by diagonal compression strut action, as shown in Fig. 1. All horizontal shear force may be transferred by the diagonal strut because the unbonded tendons transfer no shear to the joint by bond action. This should result in a significant reduction in requirements for horizontal joint shear reinforcement.

It was expected that these benefits might be offset to some extent by the high compression strains expected in the beam plastic hinge regions, which might necessitate special confinement reinforcement. The use of double interlocking spirals in the compression zones of beam plastic hinges, as shown in Fig. 2, was recommended. Ref. 1 includes a design example to illustrate the practical application of the concept.

In order to test the design assumptions about hysteretic characteristics, beam and joint shear design advantages, as well as reduced residual displacement and stiffness degradation, a
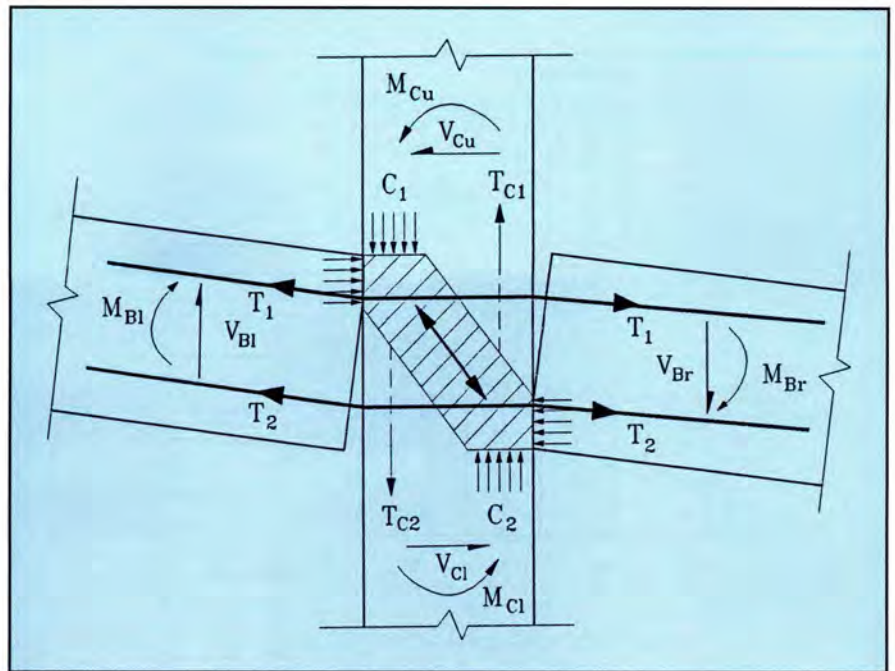

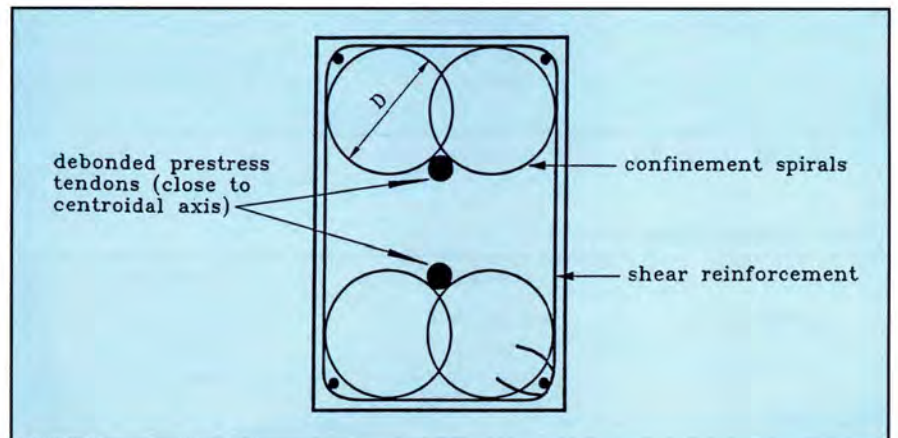Fig. 1. Forces contributing to joint shears.

Fig. 2. Beam end details.

pilot experimental program involving construction and testing of two large-scale beam-to-column subassemblages was carried out. Details of the test program and its results are summarized in the following. More complete information is available in Ref. 2.

TEST UNIT DESIGN

The two test units were taken to represent typical interior and exterior beam-to-column joints, respectively, of a perimeter one-way precast frame with continuous columns and beams connected to the columns by ungrouted post-tensioned tendons. The test units modeled the region from midcolumn height below the joint to midcolumn height above the joint and from midspan to midspan of beams on either side of the joint. Physical dimensions and reinforcement details, as shown in Fig. 3, are intended to represent prototype dimensions at a two-thirds scale. Thus, a prototype story height of 4.12 m (13 ft 6 in.) and bay length of 7.31 m (24 ft) are envisaged.

The 813 x 406 mm (32 x 16 in.) beams were prestressed with two 1200 kN (270 kips) ungrouted 12 x 12.77 mm (0.50 in.) tendons post-tensioned to $0.55f_{pu}$ after losses, providing an axial prestress of 7.2 MPa (1044 psi). For the exterior joint unit, a 500 mm (20 in.) beam stub was provided at the back of the joint for the prestressing anchorages.
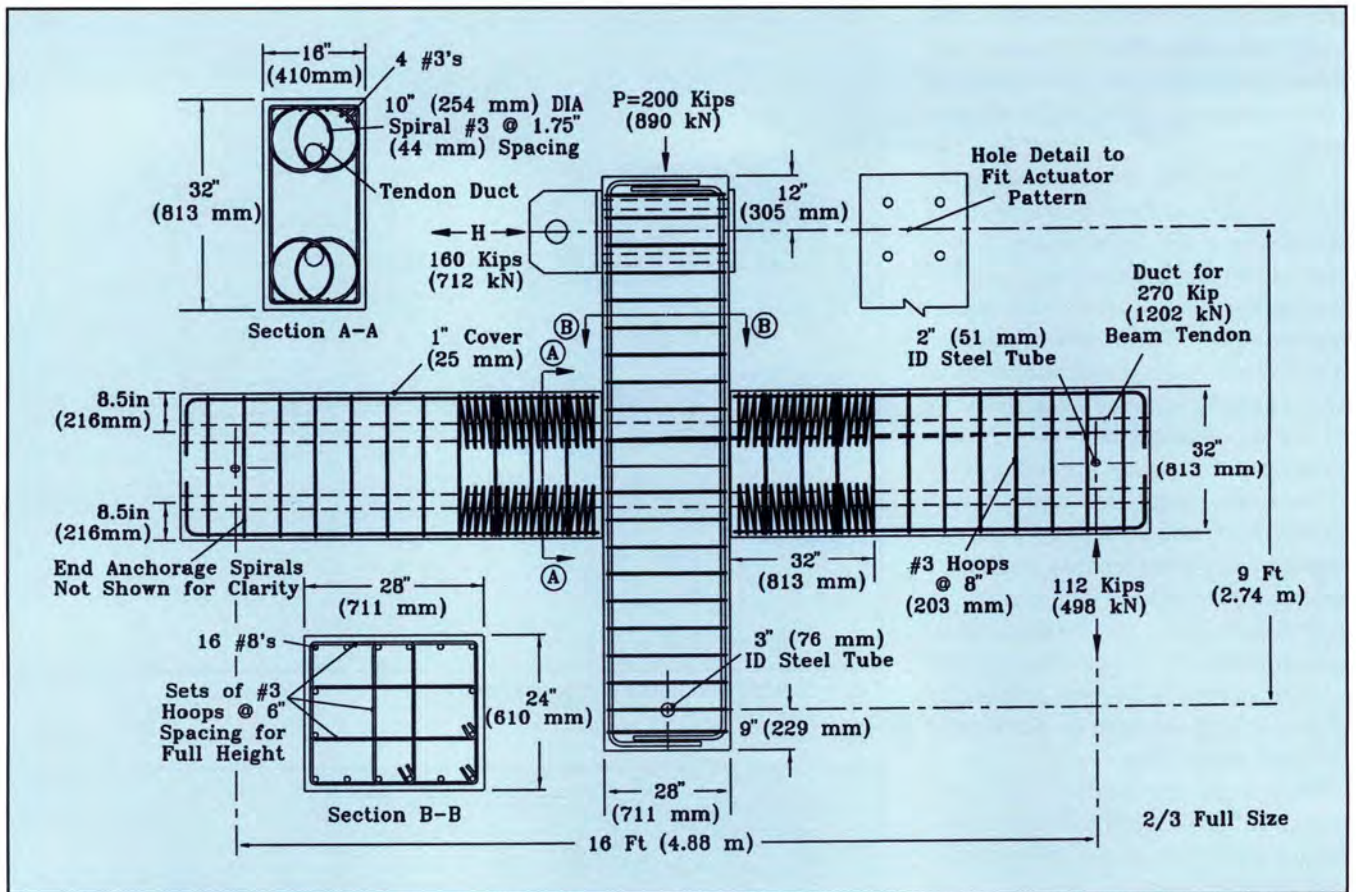
Fig. 3a. Test unit details; interior subassemblage.

Table 1. Material properties.

	Interior	Exterior
Concrete: f'_c	44.1 MPa (6.39 ksi)	45.8 MPa (6.64 ksi)
Concrete: f'_{cc} *	75.2 MPa (10.91 ksi)	77.2 MPa (11.2 ksi)
E_c †	30.5 GPa (4416 ksi)	29.1 GPa (4220 ksi)
Prestress Nominal f_{pu}	1860 MPa (270 ksi)	
Reinforcing steel:		
D10 (#3)	f_y = 462 MPa (67 ksi)	f_u = 707 MPa (102.6 ksi)
D12.7 (#4)	f_y = 448 MPa (65 ksi)	f_u = 679 MPa (98.5 ksi)
D25.4 (#8)	f_y = 452 MPa (65.6 ksi)	f_u = 723 MPa (104.8 ksi)

* Calculated value for beam plastic hinges.
† Inferred from beam strains during prestressing.

In addition to the beam prestress, longitudinal beam reinforcement in the form of corner D10 (#3) Grade 60 (f_y = 414 MPa) bars were used to stabilize the beam stirrups, which were a nominal D10 (#3) closed hoop at 203 mm (8 in.) centers. Within end regions equal to the beam depth adjacent to the column faces, confinement reinforcement in the form of double interlocking spirals of D10 (#3) bars with a 254 mm (10 in.) diameter and 44 mm (1.75 in.) pitch were provided. The corresponding volumetric ratio of con-

finement within the spirals was ρ_s = 0.025, resulting in a predicted ultimate compression strain capacity of ε_{cu} > 0.03 (see Ref. 2).

Rectangular columns of section 711 x 610 mm (28 x 24 in.) were reinforced longitudinally with 16 D25.4 (#8) Grade 60 bars and sets of D10 (#3) hoops at 152 mm (6 in.) centers for the full column height, including the region through the joint. Details are shown in Fig. 3.

Calculated member capacities are provided in Table 2, based on the

measured material strengths of Table 1. Table 1 lists the unconfined compression strength of the concrete found from cylinder tests at the time of testing the beam-to-column subassemblages and the yield and ultimate tensile strength of various reinforcement sizes used in the subassemblages. The concrete compression strength within the confined double spirals in the potential beam plastic hinge regions, listed in Table 1, was calculated using the confined strength model developed by Mander et al.[3] The modulus of elasticity of the concrete was found from beam strains measured during prestress operations and agreed well with values predicted using the standard ACI equation:[4]

$$E_c = 4735\sqrt{f'_c} \text{ MPa} = 57,000\sqrt{f'_c} \text{ psi}$$
(1)

The flexural strength M_{lp} of the beam plastic hinges was based on the assumption that the cover concrete would spall off the spirals at maximum strength, but that the confined concrete within the spirals would
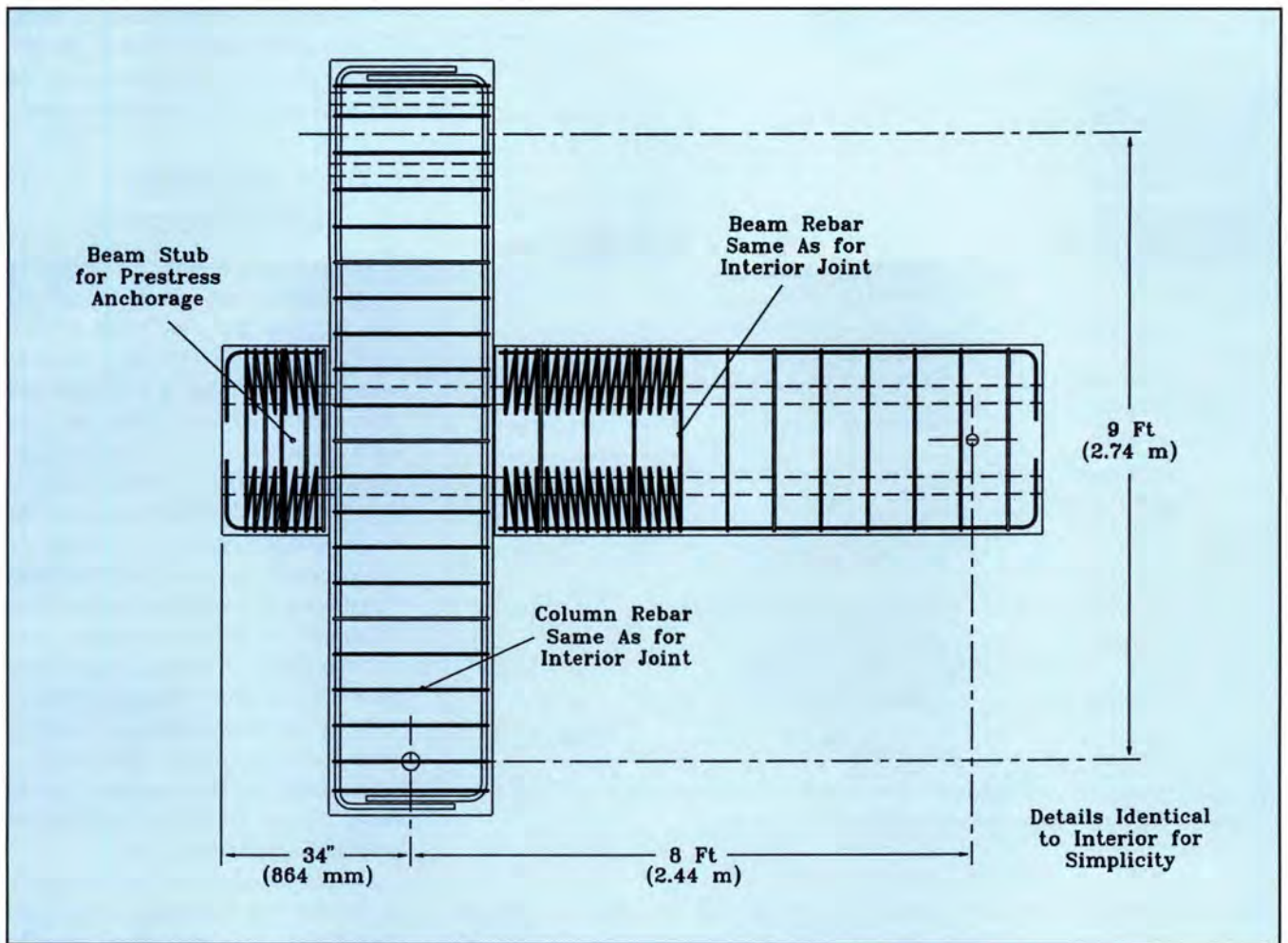
Fig. 3b. Test unit details; exterior subassemblage.

achieve the values of f'_{cc} as listed in Table 1. An equivalent rectangular stress block developed by Popovics[5] was used to determine the resultant compression force and centroidal position for a given neutral axis depth.

The beam flexural strength listed in Table 2 corresponds to the prestressing tendon being stressed to its limit of proportionality, assumed to equal $0.8f_{pu}$. This limit was the design basis for determining the strength and deformation capacity, using the procedures outlined in Ref. 1. Full details of the strength calculations are given in Ref. 2.

Various methods were used to determine the shear strength of the beams. These results are listed in Table 2. In each case, the strengths are based on measured material properties and do not include strength reduction factors. Significant differences in the design strength were obtained using the ACI design equations. This is because the formulas could apply to prestressed

concrete beams or to axially loaded members. A recently developed shear strength equation by Priestley et al.[6] gave a much higher predicted shear strength than the ACI equations. The method of Priestley et al. considers the shear strength to be provided by an additive equation of the form:

$$V_n = V_c + V_s + V_p \qquad (2)$$

where V_c is the concrete contribution, which decreases in magnitude as flexural ductility increases; V_s is a truss contribution provided by transverse reinforcement based on a 30-degree inclination of the compression strut to the member axis; and V_p is an axial load contribution whose magnitude depends on the axial load on the member and the member length to depth (aspect) ratio. The form of this equation, which provides a close prediction of a wide range of column data, should also be suitable for predicting the strength of prestressed members.

It can be seen from Table 2 that the

ACI "prestressed beam" equation provided a shear strength only 15 to 18 percent higher than the shear corresponding to flexural strength M_{lp}. Considering possible flexural overstrength and the normal use of a flexural strength reduction factor of 0.85, this indicates an inadequate margin of strength. The other two methods indicate adequate shear strength.

Column flexural strength, based on moment-curvature analysis considering the effects of confinement and a maximum compression strain of 0.005, exceeded the column moment corresponding to development of M_{lp} in the beams. The critical column moment was calculated at a position corresponding to the depth of the beam compression resultant in the plastic hinge, rather than at the nominal level at the top of the beam.

For the interior subassemblage, column flexural strength exceeds demand by 65 percent. This reflects the results of a capacity design process that con-

Table 2. Member forces and capacities.

	Interior	Exterior
Beam flexure		
Beam prestress after losses	2634 kN (592 kips)	2670 kN (600 kips)
Beam flexural strength M_{lp}*	1042 kN-m (9225 kip-in.)	1033 kN-m (9145 kip-in.)
Beam shear		
Shear corresponding to M_{lp}	500 kN (112.4 kips)	496 kN (111.4 kips)
V_n (ACI, prestressed beam)	582 kN (131 kips)	588 kN (132 kips)
V_n (ACI, column)	670 kN (150.5 kips)	681 kN (153.1 kips)
V_n (Priestley[6])	955 kN (214 kips)	962 kN (216 kips)
Column flexure		
Axial force P	980 kN (200 kips)	0
Moment corresponding to M_{lp}	957 kN-m (8470 kip-in.)	469 kN-m (4160 kip-in.)
M_n (moment-curvature analysis)	1576 kN-m (13,900 kip-in.)	1413 kN-m (12,500 kip-in.)
Column shear		
Shear corresponding to M_{lp}	890 kN (200 kips)	440 kN (99 kips)
V_n (ACI, column)	930 kN (209 kips)	872 kN (196 kips)
V_n (Priestley[6])	1550 kN (349 kips)	1350 kN (303 kips)
Joint shear		
Horizontal shear force V_{jh}	2630 kN (592 kips)	‡
Vertical shear force V_{jv}	3011 kN (677 kips)	‡
Shear stress V_j	$0.92\sqrt{f_c'}$ MPa $(11\sqrt{f_c'}$ psi)	‡
Hoop shear capacity	656 kN (147 kips)	‡
Drift†	0.0256	0.0182

* Calculated at steel limit of proportionality.
† Story drift at steel limit of proportionality.
‡ Standard calculations for joint shear inappropriate due to prestress anchorage.

siders the effects of moment over-strength in the beam plastic hinges and dynamic amplification due to higher mode effects.[7] Column details for the exterior subassemblages were kept the same as for the interior subassemblage, resulting in a higher ratio of strength to demand for that unit.

Column shear force corresponding to development of M_{lp} in the beam plastic hinges was 890 and 440 kN (200 and 99 kips) for the interior and exterior subassemblages, respectively. These values are also the predicted lateral strength of the units in terms of applied lateral force. The shear strength of the columns, using the ACI design equations with measured material properties and a strength reduction factor of $\phi_s = 1.0$, indicated a marginal strength for the interior subassemblage, but an adequate strength for the exterior unit. The method of Priestley et al.[6] indicated a substantial reserve of shear capacity.

Table 2 lists joint shear forces for the interior subassemblage. The shear stress at development of M_{lp} in the beam hinges was 6.07 MPa (881 psi), which corresponds to $0.14f_c'$ or $0.917\sqrt{f_c'}$ MPa

$(11.0\sqrt{f_c'}$ psi). The shear strength provided by the five horizontal stirrup sets within the joint region was only 25 percent of the horizontal shear force. In fact, it is doubtful that the top and bottom stirrup sets could be considered effective because they were located outside the centroid of the beam compression force and, hence, are technically outside the true joint region.

This would reduce the capacity provided by the transverse reinforcement to 15 percent of the total joint shear. However, it was expected that the introduction of the horizontal joint shear solely by beam compression stress resultants would lead to an efficient diagonal strut carrying the entire horizontal shear force, as discussed previously in Ref. 1. Mechanisms involved in the joint shear transfer are discussed in more detail later in this paper, based on experimental results.

Values for the joint shear force for the exterior unit are not listed in Table 2 because the influence of the distributed horizontal compression force at the back of the joint, provided by anchorage of the prestressing tendons, makes the calculation of joint shear

forces and stresses by traditional methods inappropriate. However, experimental results are used to clarify the behavior of this unit later in the paper.

TEST UNIT CONSTRUCTION

The columns, beams, and beam stub for the interior and exterior units were precast from the same batch of concrete. At an age of 18 days, the units were connected with a thin layer, approximately 6.5 mm (¼ in.) thick, of epoxy grout with a light prestress applied to the beams to ensure even seating. Note that the end surfaces of the beams and the connecting surfaces on the columns were not specially prepared prior to connection beyond wire brushing to remove excess laitance.

No mild steel reinforcement connected the beams with the columns. Twenty-one days after casting, the beams were prestressed with measurements taken of beam surface strains using 200 mm (8 in.) gauge length demountable mechanical gauges.

For convenience, the test units were assembled and prestressed in the horizontal plane and later rotated into the vertical plane for testing.

TEST SETUP AND TESTING SEQUENCE

The experimental setup for the interior subassemblages is shown in Fig. 4. Lateral displacements were applied at column midheight above the joint, with the unit rotating about a pin in the column at the lower column midheight. The beams at midspan positions were connected by pin-ended links to the strong floor, allowing free lateral translation of the beams but restraining vertical movement and ensuring a moment pattern in the subassemblage similar to that in a joint of a building frame.

The interior test unit was subjected to an axial load of 890 kN (200 kips), which was felt to be a minimum representative axial load level. A low level was used to ensure that joint conditions were critical because a higher axial load was expected to improve the force transfer within the joint.[7] Because of expected seismic axial force variations in
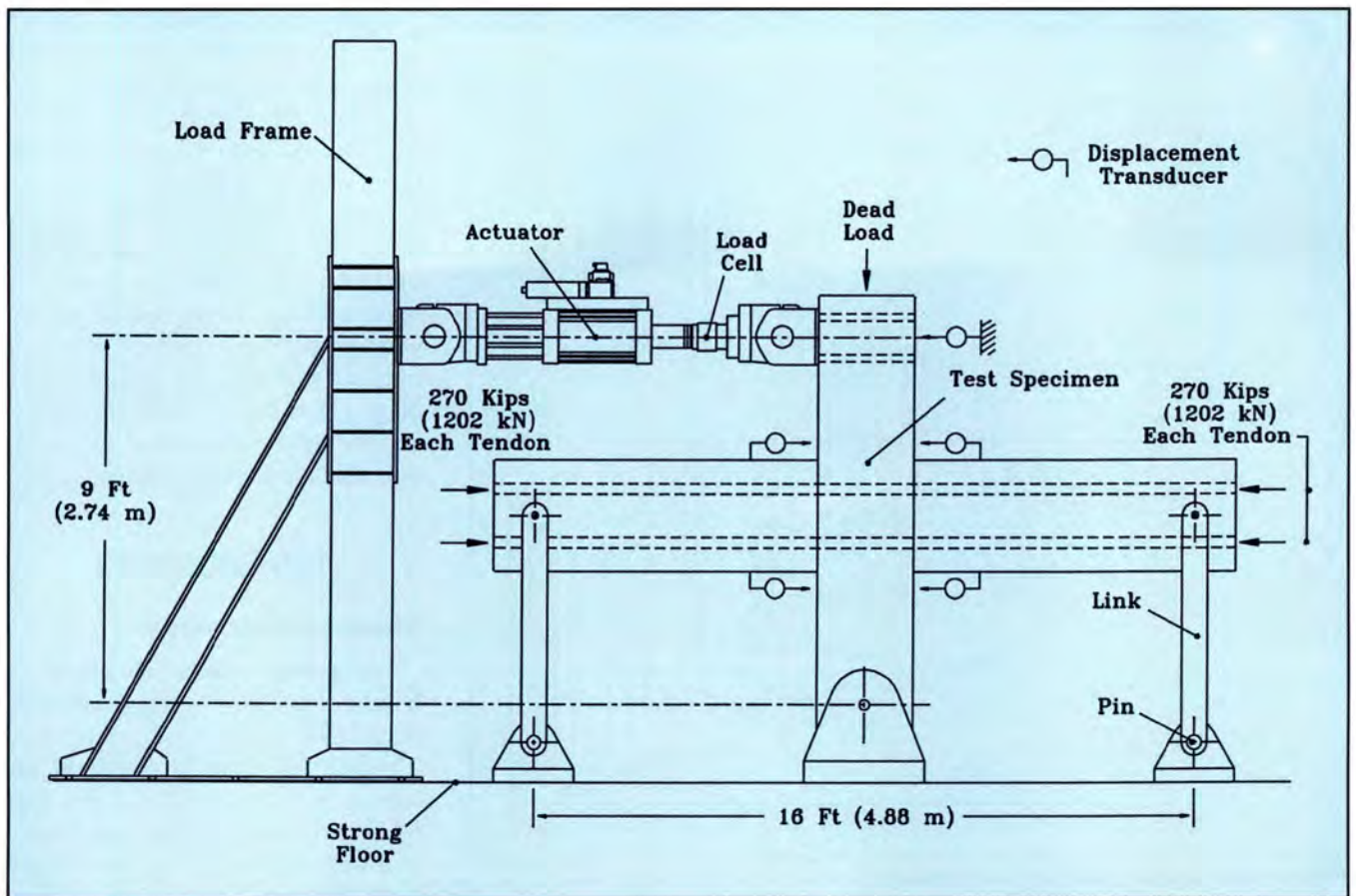
Fig. 4a. Elevation of interior subassemblage test setup.

the exterior unit, no axial load was applied, though a more realistic regime would have varied the axial force simultaneously with the applied lateral force.

Due to a test design error, the pin at the base of the column was undersized. As a consequence, there was significant deformation of the pin under axial and lateral load, particularly for the interior joint unit. This resulted in additional flexibility in the test unit in the elastic stages of response and resulted in bending moments being developed in the beam of the interior unit by the column axial load. These bending moments induced tension stresses at the beam soffits and resulted in nonlinearity of response under lateral displacements occurring earlier than predicted.

The patterns of applied displacements and forces for the two units are shown in Fig. 5. These followed the standard test pattern used in the U.S./PRESSS program,[8] which is based on increments of drift such that displacements at a given level are never more than 50 percent higher than those at the previous level. At each level,

three full cycles of drift are applied. The test pattern is based on drift rather than ductility increments because ductility can be difficult to define for systems incorporating components other than conventional reinforced concrete or mild steel components.

Because the test units were designed to have drift capacities of at least 2 percent, testing was continued significantly past this limit to ensure an adequate reserve of displacement capacity. In the case of the interior unit, the maximum applied drift of 2.8 percent was dictated by the displacement capacity of the transducer monitoring column-top lateral displacement. For the exterior unit, a transducer with greater displacement range was used and testing was taken up to 4 percent drift.

INSTRUMENTATION

The test program was considered to be a pilot program designed to investigate the feasibility of the design procedures outlined in Ref. 1. As a consequence of the limited funding available for the tests, a comparatively
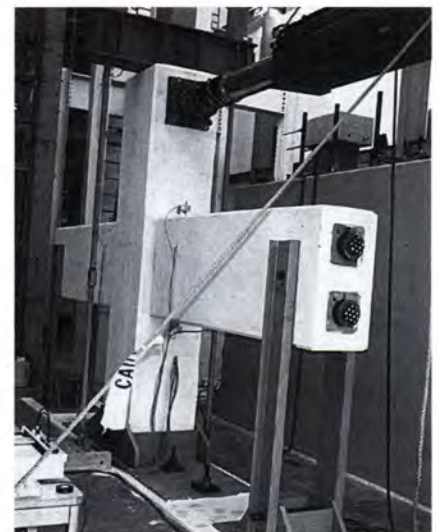

Fig. 4b. Photograph of interior subassemblage test setup.

modest instrumentation was used. In addition to the usual measurements of actuator force and column top displacement, the three beam stirrups closest to the column face and the five column hoop sets within the joint region were gauged with electric resistance strain gauges, with one gauge on every leg of the hoops or stirrups.
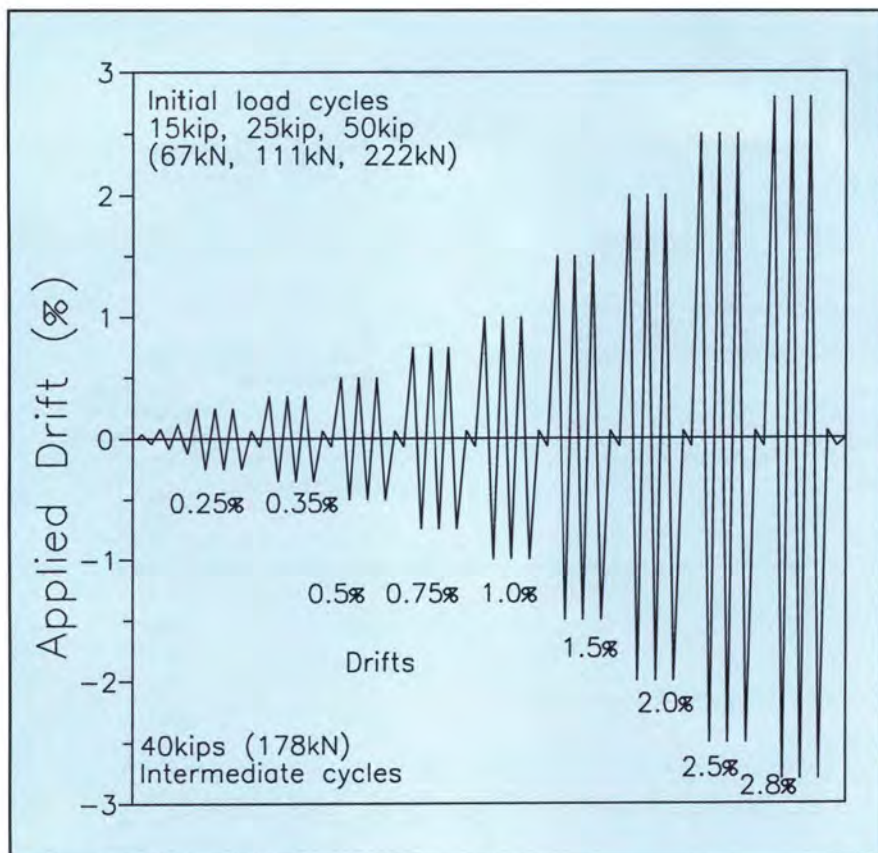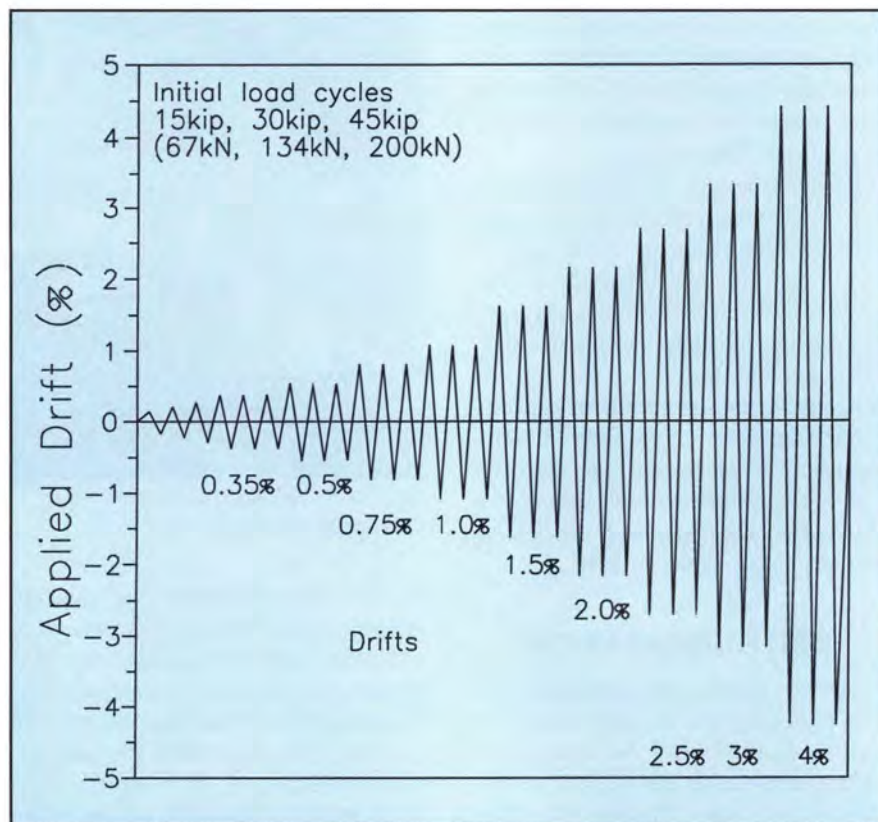
Fig. 5a. Test regimes; interior subassemblage.

Fig. 5b. Test regimes; exterior subassemblage.

Displacement transducers attached to the top and bottom surfaces of the beams 150 mm (6 in.) from the column face and measuring onto the column face enabled surface strains in the beam plastic hinge region to be estimated by interpolation between the gauge lengths. These were centered 50 mm (2 in.) above or below the beam surface. At high drift angles, compression surface strain was estimated from the measured strain 50 mm (2 in.) above the beam surface, and the theoretical neutral axis position, using linear interpolation.

TEST RESULTS

Visual Observations

Figs. 6 and 7 show conditions of the interior and exterior subassemblages, respectively, at the design limit of 2 percent drift and at maximum response. For the interior unit (see Fig. 6), beam flexural cracking was limited to a single wide crack at the column face. Horizontal splitting cracks associated with spalling of cover concrete in the beams first developed at a drift of 0.75 percent, and spalling increased as drift increased.

At the design drift limit of 2 percent, the spalling of cover concrete extended about 200 mm (8 in.) from the column face. At maximum drift of 2.8 percent, spalling extended back about 300 mm (12 in.) from the column. Very little other damage to the beams occurred, except for minor horizontal cracks initiating at the column face, which were caused by incompatibility of curvature on the compression and tension surfaces of the beam in the plastic hinge region.

The extent of beam damage at maximum drift is much less than would be expected of an equivalent monolithic reinforced concrete subassemblage.

Column flexural cracking initiated at a drift of 0.35 percent, outside, and also within the joint region. At a drift of 0.5 percent, considerable inclined joint shear cracking developed. This extended until a drift level of 1.0 percent; the crack pattern stabilized and few further cracks developed at higher drifts. As can be seen from Fig. 6b, the joint cracks were well distributed and
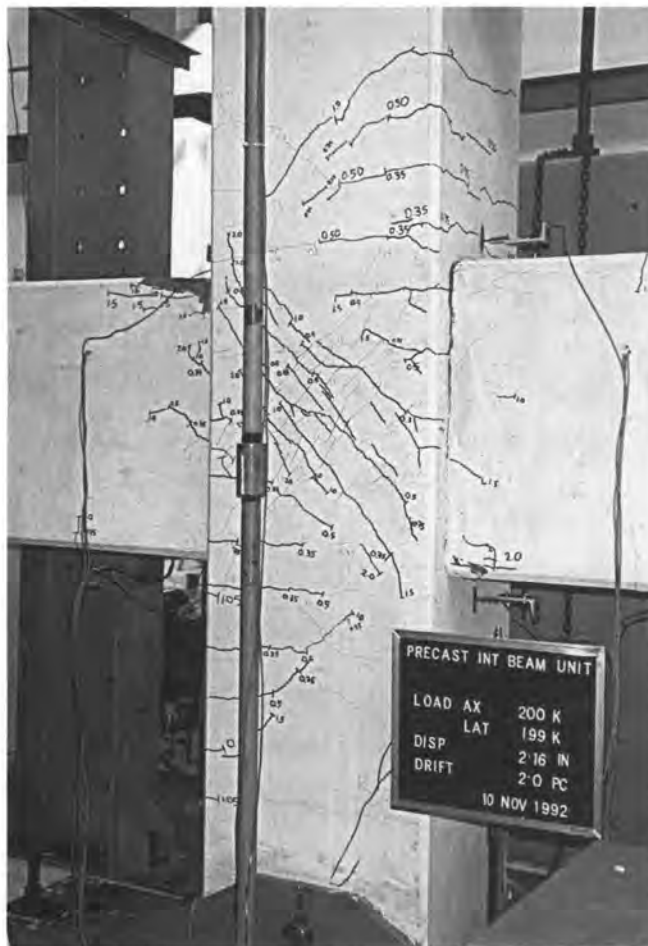
Fig. 6a. Interior subassemblage crack patterns at design and maximum drift. Design drift = 2 percent.
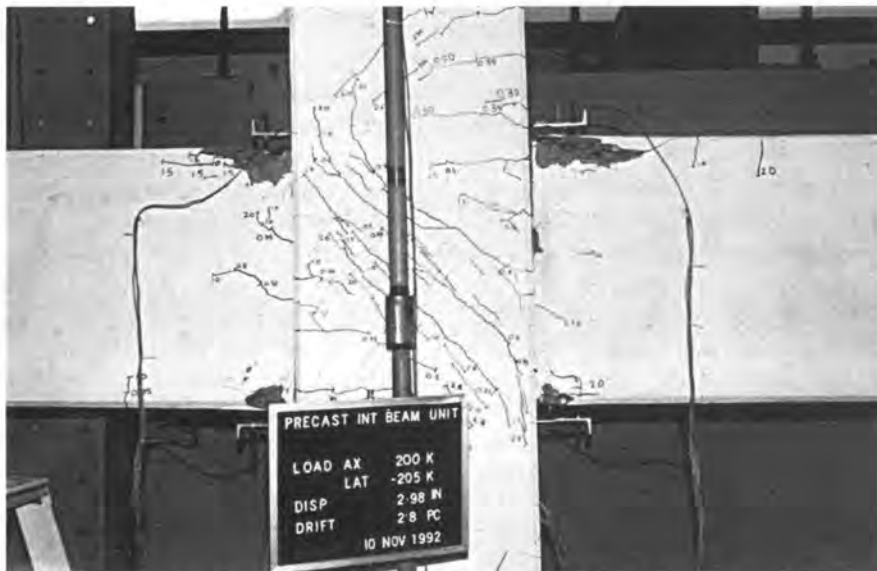

Fig. 6b. Interior subassemblage crack patterns at design and maximum drift. Maximum drift = 2.8 percent.

oriented approximately parallel to the corner-to-corner diagonal, though the inclination was flatter in the center of the joint and steeper towards the ends of the diagonal strut.

The exterior joint subassemblage displayed a similar lack of damage to the interior unit. At the design drift level of 2 percent, very minor spalling occurred and at 4 percent drift, the surface spalling extended about 300 mm (12 in.) from the column face. It was evident that the double interlocking spirals were very effective in confining the beam compression zones and maintaining the integrity of the plastic hinge regions.

It was also evident that the spirals extended an unnecessary length into the beam and a length of half the beam depth [i.e., 400 mm (16 in.)] would have been adequate. Joint shear cracking started to develop at a drift of 0.5 percent and continued to extend and develop up to a drift of 2.0 percent, after which it stabilized. The joint cracks were inclined closer to the horizontal than with the interior joint and were noticeably finer.

Lateral Force-Displacement Hysteresis Response

The lateral force-displacement hysteresis response for the two units is shown in Fig. 8, together with the computed simplified force-displacement envelope calculated in accordance with the approach suggested in Ref. 1. The theoretical envelopes only extend to the drift corresponding to development of the prestress limit of proportionality strain of 2.6 and 1.8 percent for the interior and exterior units, respectively.

The experimental response indicated a stable hysteretic response with comparatively little strength degradation between successive cycles to a given drift level. The loops appear a little irregular due to the deformation of the bottom support pin (as noted earlier), some slop in the pins of the beam links, and also due to minor control problems with the actuator. Because all other actuators in the test laboratory were committed to other experiments, it was necessary to use a 2.67 MN (600 kips), 900 mm (36 in.) travel actuator for the tests. This resulted in poor control at the low force and displacement levels required of the test, particularly for the exterior joint (see Fig. 8b).

The predicted force-displacement response is a reasonable envelope of the experimental response. Due to reasons explained above, the initial stiffness was less than the theoretical pre-

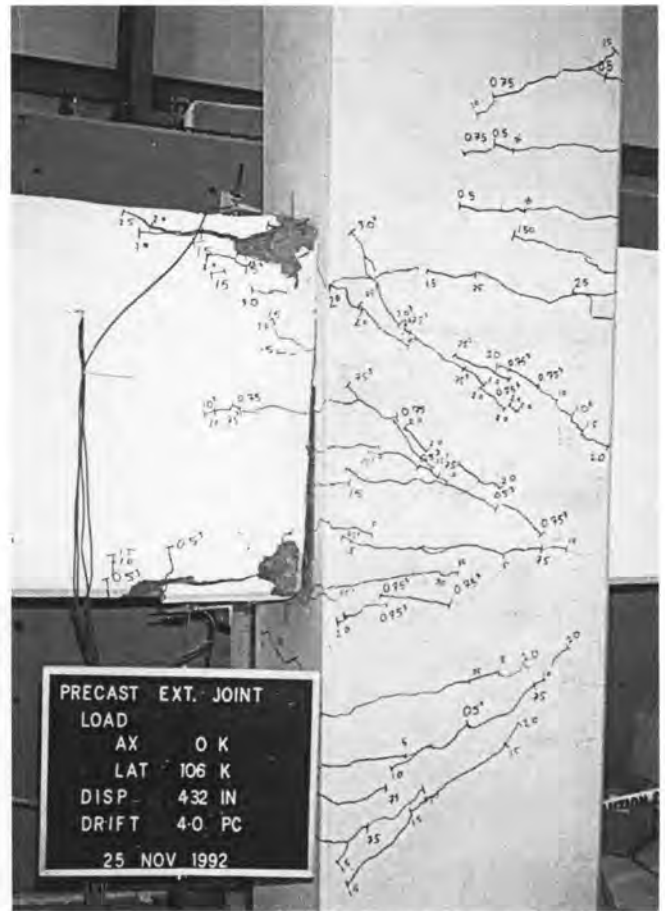Fig. 7a. Exterior subassemblage crack patterns at design and maximum drift. Design drift = 2 percent.

Fig. 7b. Exterior subassemblage crack patterns at design and maximum drift. Maximum drift = 4 percent.

diction, but the post-yield response stiffness agrees well with the theoretical value. The maximum strength for the interior joint was 3 percent higher than the predicted value, while the exterior joint attained maximum force levels about 8.5 percent, on average, above the predicted strength at the limit of proportionality.

The theoretical idealization of response from Ref. 1 implied a bilinear elastic response, whereby the subassemblages should unload down the loading force-displacement curve, implying zero hysteretic energy absorption. It is clear that this behavior was not observed in the tests. The units tended to unload down a line of somewhat reduced stiffness on the first cycle to a given drift, and then reload and unload down the same line on subsequent cycles. As expected, however, residual drifts were small at all levels of response.

Fig. 9a shows the residual drift as a function of maximum drift level for the interior subassemblage and com-

pares this with a straight line approximation with a 2.2 percent slope, which provides an adequate estimate of residual drift. Thus, after a maximum drift of 2 percent, corresponding to the design limit, residual drift was about 0.044 percent. This can be compared with typical residual drifts for reinforced concrete subassemblages of about 50 percent of peak drift.

The theoretical response from Ref. 1 also assumed that the beam prestress would result in stiffness at low lateral force levels being equal to the initial uncracked stiffness, even after inelastic response. As is apparent from Fig. 9b, this is also incorrect, because stiffness decreases at the design limit of 2 percent drift to about 35 percent of the initial value. However, this is again substantially higher than would be expected of a reinforced concrete subassemblage that had been subjected to similar drifts.

Alternative hysteretic models that better describe the force-displacement response than that suggested in Ref. 1

are shown in Fig. 10. The first is a relatively simple zero residual displacement model where unloading is always directed towards the origin and loading or reloading occurs along the envelope curve or the previous unloading curve. It is apparent that the model of Fig. 10b, where unloading is to a point with residual displacement of α times the maximum drift ($\alpha = 0.022$ for these tests) would provide an improved estimate of response. The numbering sequence in the loops of Fig. 10 is intended to represent a response to an arbitrary input.

Beam Compression Strains Plastic Hinge Region

Extreme fiber compression strains in the end 150 mm (6 in.) of the beam adjacent to the column face are shown in Fig. 11 as a function of the test unit drift. Significant and consistent differences were recorded between the strains on the top surface and bottom surface of the beam, with top strains
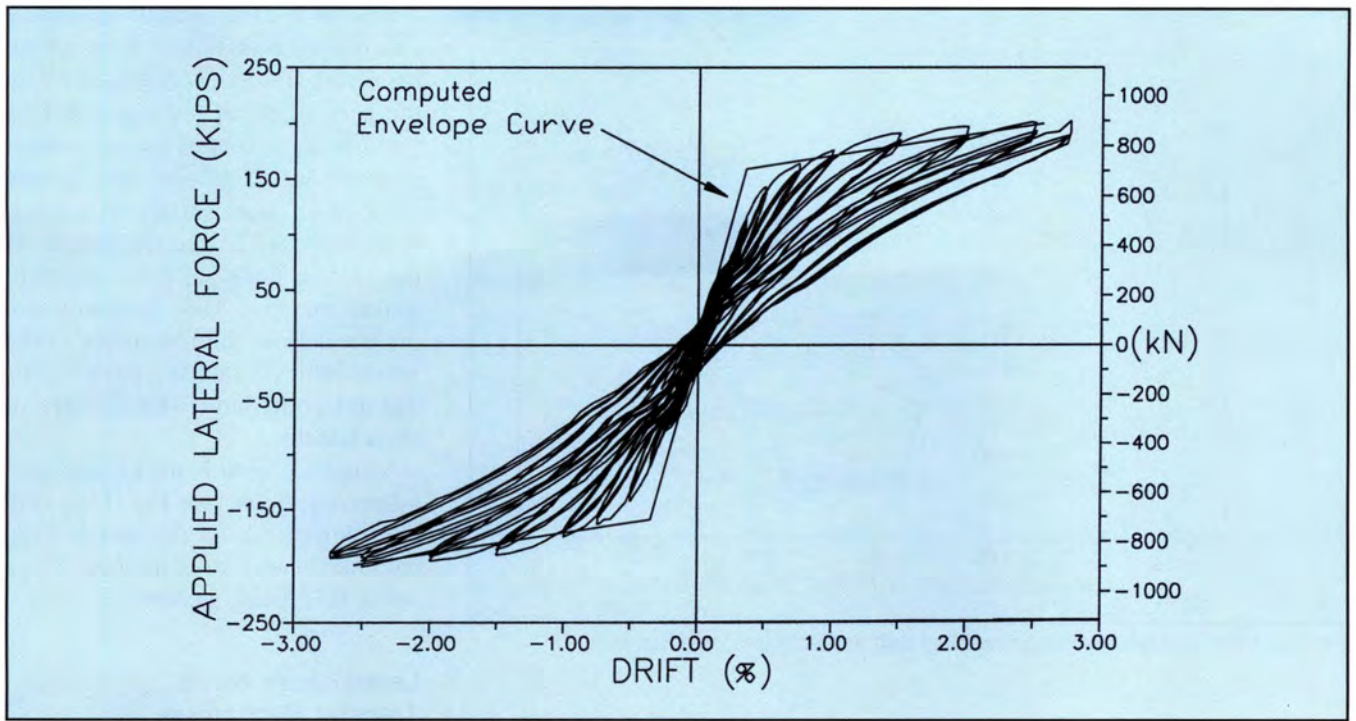
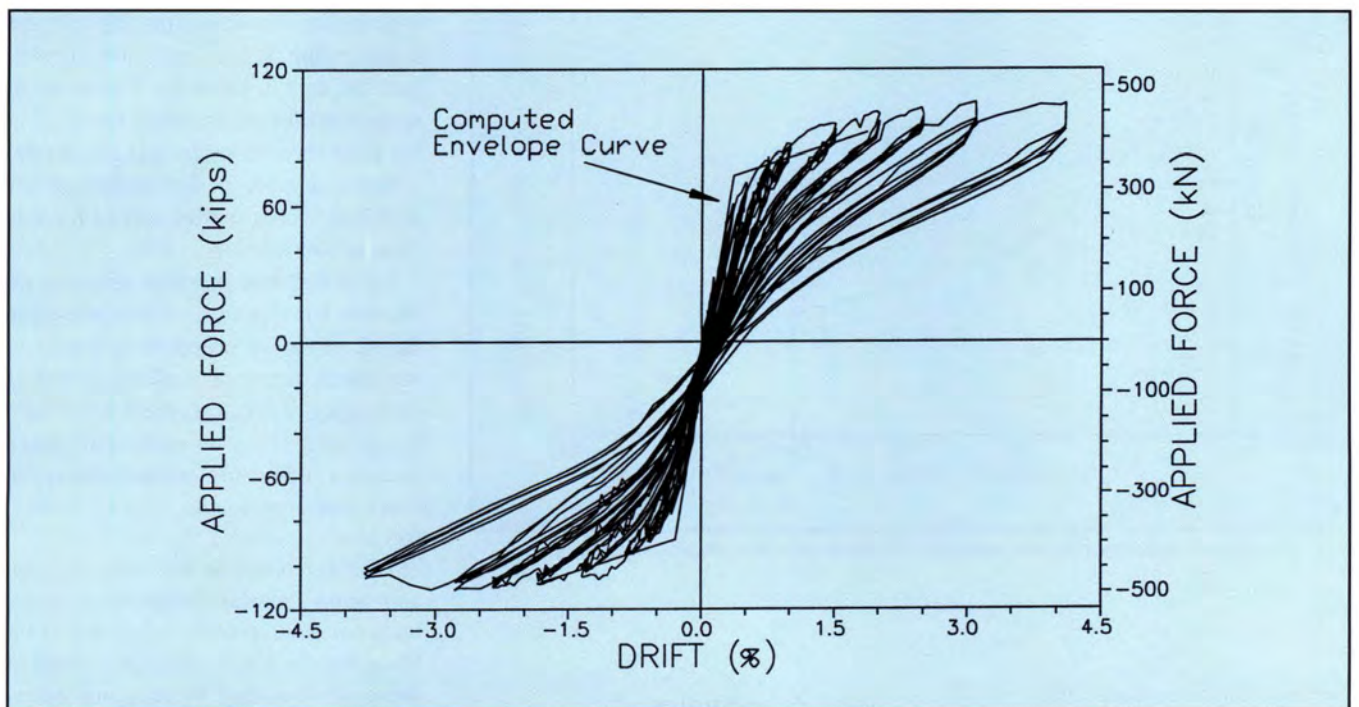Fig. 8a. Lateral force-displacement response; interior subassemblage.

Fig. 8b. Lateral force-displacement response; exterior subassemblage.

about twice those on the bottom surface. It is not clear what caused these differences or whether or not they are systematic differences. Peak strain levels averaged about 2 percent at 2 percent drift, but increased at a more rapid rate than the drift increase.

Beam Hoop Strains

In all cases, strains recorded on the transverse reinforcement in the beams were extremely low and generally compressive. It was thus obvious that the transverse reinforcement was not

required to participate in shear transfer, even within the beam plastic hinge region. Typical results for one beam of the interior subassemblage are shown in Fig. 12. Here, strains vary between -125×10^{-6} and 45×10^{-6} with compressive strains being highest at the
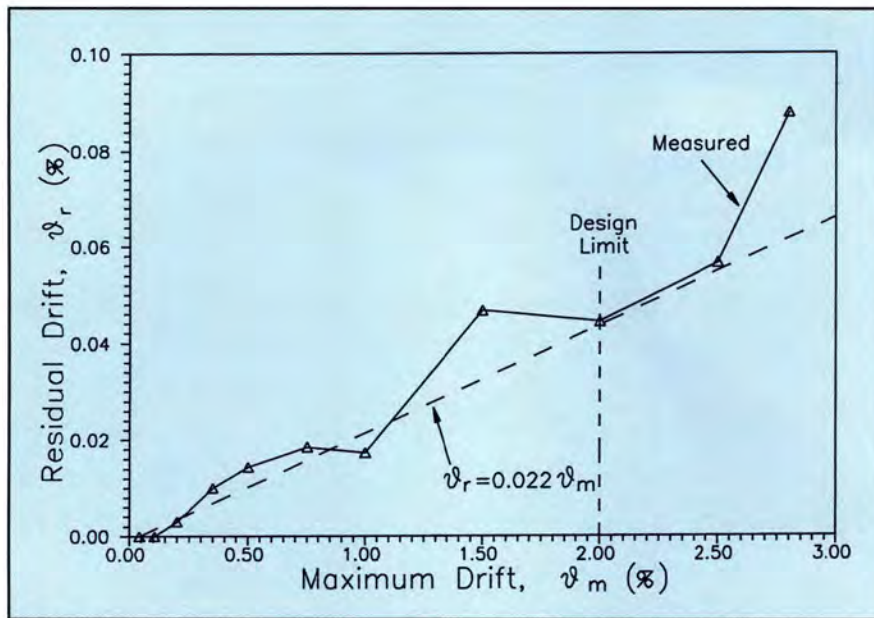
Fig. 9a. Interior subassemblage residual drift and stiffness; residual drift.
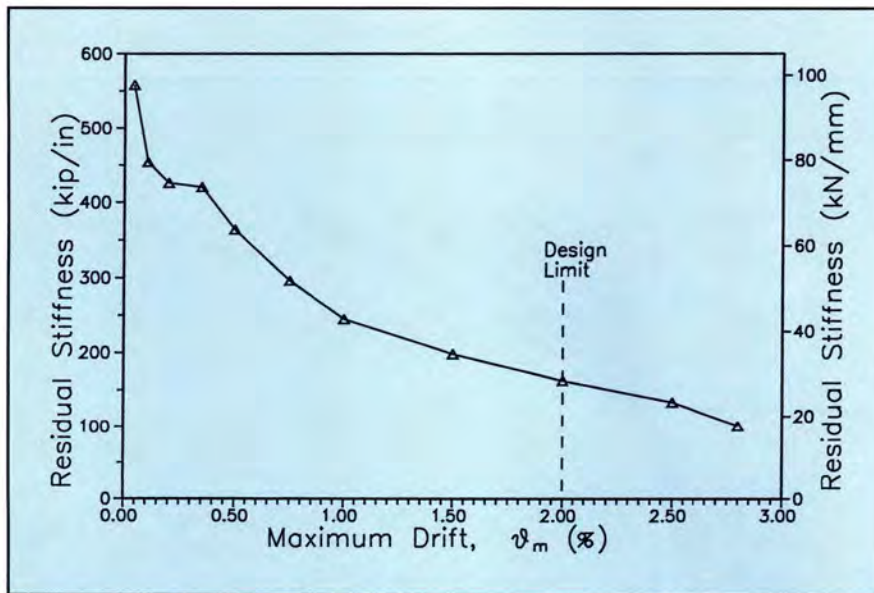

Fig. 9b. Interior subassemblage residual drift and stiffness; residual stiffness.

center of the three hoop sets.

This behavior agrees with the mechanism described earlier to explain the short horizontal cracks near midheight of the beam, initiating at the column face. This mechanism involved incompatible curvatures on the compressive and tensile surfaces of the beam, resulting in vertical strains that must be tensile at the column face and (for equilibrium) compressive some distance away.

Joint Hoop Strains

Strains developed in the hoop sets within the joint region are shown in Fig. 13 for different drift levels. Two plots, one for low drifts and the other for high drift levels, are shown for the interior subassemblage. Data are only presented for high drift levels of the exterior subassemblage because strains were very low at early stages of testing.

Results for the interior joint indicate that the central three hoop sets all sustained strains exceeding yield in the later stages of testing, with first yield being recorded by the central hoop set at 0.75 percent drift. Strains close to $4\varepsilon_y$ were sustained at maximum response. Although gauges of the bottom hoop set failed prior to testing, the upper hoop set results and the trend from the remainder of the hoops indicate that the outer hoops did not contribute significantly to shear transfer.

Strains recorded in the exterior subassemblage joint (see Fig. 13c) were much lower than for the interior joint, with maximum values of about 700 x 10^{-6} or $0.3\varepsilon_y$ being attained.

Lateral Joint Force Transfer Mechanism

It would appear that slightly insufficient transverse hoop reinforcement was provided for the interior joint, while excess reinforcement was provided for the exterior joint. It is of interest to investigate the data in more detail in order to understand the mechanisms involved in the joint shear transfer, and also to develop a suitable design approach for joint transverse reinforcement for this form of construction.

Fig. 14 shows possible strut-and-tie models for the two subassemblages based on the recorded hoop forces at maximum response. Column forces at each layer of reinforcement have been calculated from moment-curvature analyses, using the column moments corresponding to the applied lateral force.

With reference to Fig. 14a, column and beam flexural compression resultants combine to form a diagonal strut. Hoop tensile forces are equilibrated at the core boundary by diagonal struts angling towards the centroid of the beam and column compression resultants and by changes in the vertical forces in the column reinforcing bar outer layer. Because the angle of these struts differs between hoop layers, the efficiency in facilitating column force transfer by bond also varies.

The implication of these variable angle struts is that cracking within the joint should not be by a series of
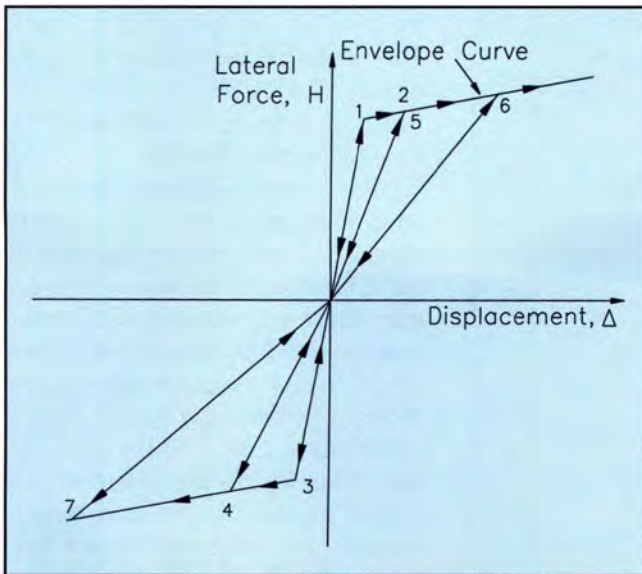
Fig. 10a. Possible force-displacement models for prestressed ungrouted beam-to-column subassemblages; zero residual displacement model.
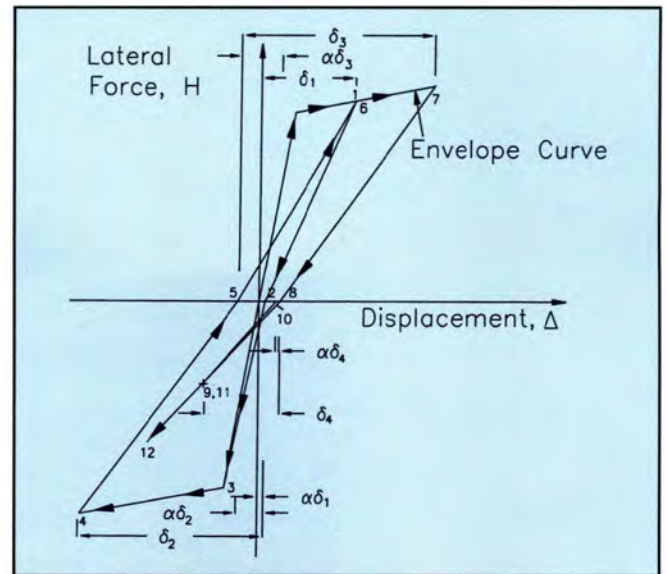

Fig. 10b. Possible force-displacement models for prestressed ungrouted beam-to-column subassemblages; proportional residual displacement model.
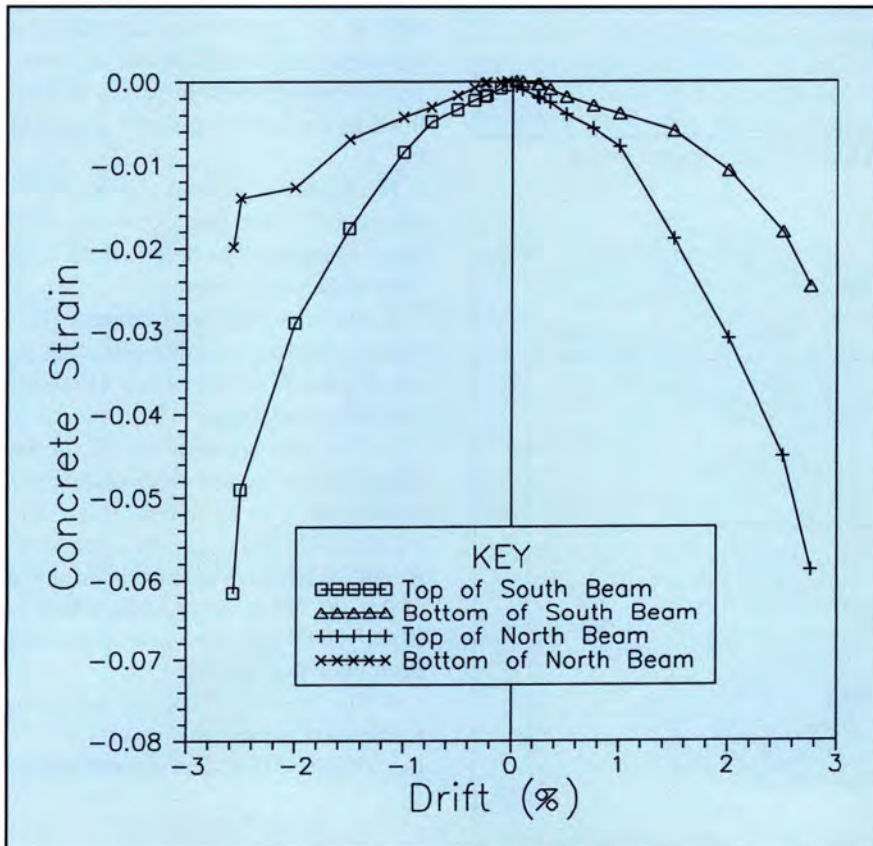

Fig. 11a. Extreme fiber compression strains in beam plastic hinges; interior subassemblage.

cracks, each parallel to the corner-to-corner diagonal, but by cracks with an inclination tending towards the horizontal as distance from the corner-to-corner diagonal increases. This is supported by the observed crack patterns of Figs. 7 and 8.

Based on this model, it is possible to determine how much of the net force differential in the outer layer of column bars was transferred by strut-and-tie action involving the hoop sets and how much was transferred by bond within the major diagonal strut

formed by beam and column flexural compression results. It is assumed at this stage that the force differential in the inner layers of column bars is directly transmitted to the major strut.

From Fig. 14a, the force differential in the outer layer of column bars is 668 + 272 = 940 kN (211.5 kips). As shown in Fig. 14a, hoop forces assist in transferring only 96 + 62 + 26 = 184 kN (41.3 kips) or 19.5 percent of the total force. It is inferred that the remainder, $\Delta T = 940 - 184 = 756$ kN (170.2 kips), was transferred by bond within the width of the diagonal strut.

It is instructive to compare the force ΔT that could be transferred by bond within the depth of the beam ultimate compression zone (as an indication of the effective vertical width of the diagonal strut) with the observed value. Thus:

$$\Delta T = \Sigma_o u_u c \qquad (3)$$

where

Σ_o = surface area per unit length of four D25.4 (#8) bars

Σ_o = 319 mm^2/mm (12.56 sq in./in.)

c = calculated depth of beam ultimate compression zone = 154 mm (6.08 in.)

u_u = ultimate bond stress = $K\sqrt{f_c'}$

With $\Delta T = 756$ kN (170.2 kips), Eq. (3) yields $u_u = 15.4$ MPa (2229 psi). For $f_c' = 44$ MPa (6390 psi), this results
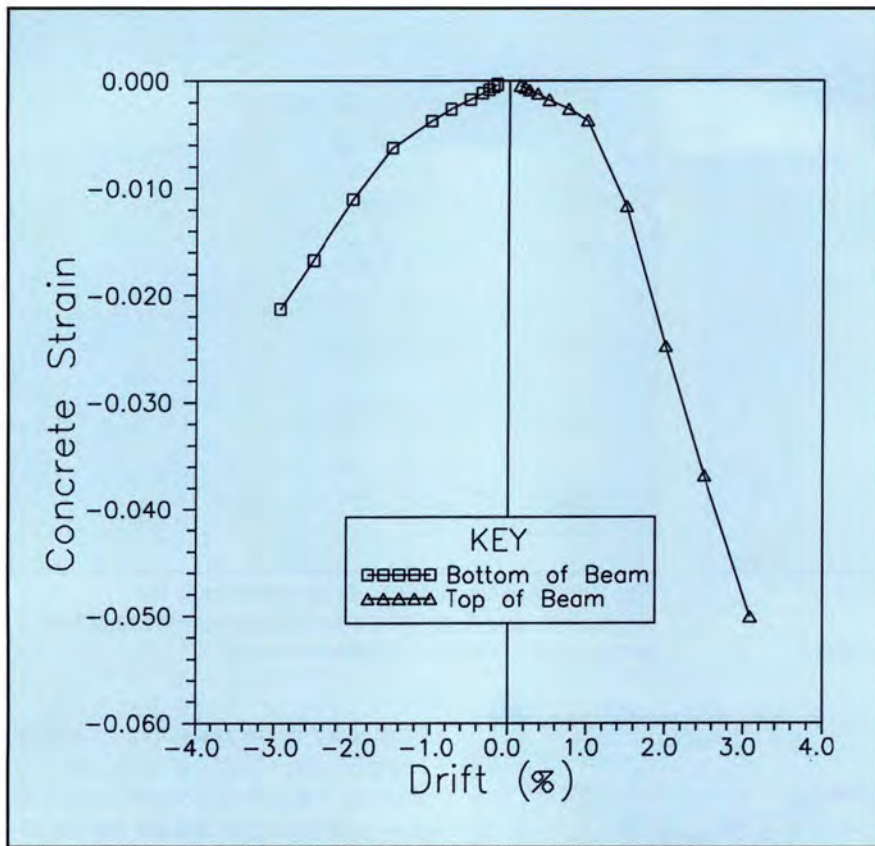
Fig. 11b. Extreme fiber compression strains in beam plastic hinges; exterior subassemblage.
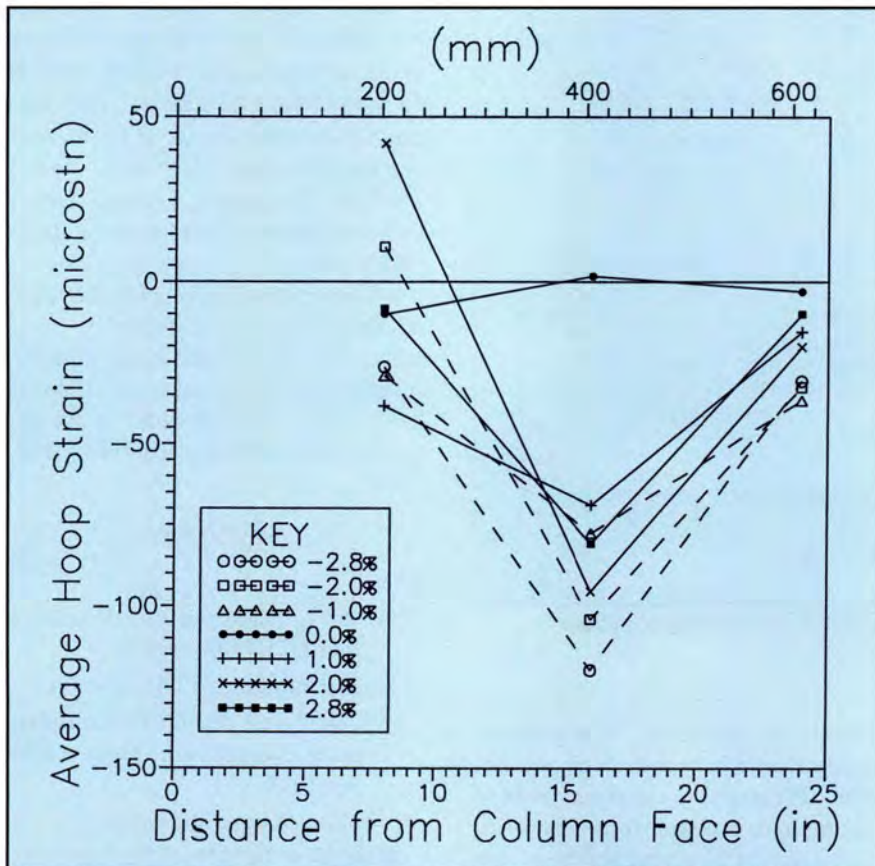

Fig. 12. Strains in beam transverse reinforcement; interior subassemblage south beam.

in $u_u = 2.32\sqrt{f_c'}$ MPa ($27.9\sqrt{f_c'}$ psi). This is close to ultimate bond stresses of $2.5\sqrt{f_c'}$ MPa ($30\sqrt{f_c'}$ psi) for confined concrete situations reported by Eligehausen[9] and Priestley.[7]

Using a similar approach for the exterior joint unit in Fig. 14b, it would appear that very little of the force in the critical outer column reinforcement layer was transmitted by strut-and-tie action involving transverse hoops. Using the same approach as above, it is found that $u_u = 15.9$ MPa (2310 psi) or $2.36\sqrt{f_c'}$ MPa ($28.3\sqrt{f_c'}$ psi). Thus, results are obtained very similar to those for the interior unit despite very different column moments, axial force levels, and column reinforcing bar stress levels. This would appear to provide some credence to the proposed mechanism.

The above argument leads to a possible design approach to determine the required minimum amount of transverse reinforcement in joints, as outlined in the following steps, related to Fig. 15:

1. The beam neutral axis depth is calculated. If the beam ends are confined, this should be based on the confined strength of concrete.

2. The distribution of column reinforcing bar forces corresponding to maximum feasible beam flexural strength is calculated.

3. The incremental force ΔT_1 in the outer layer of column bars transferred within the joint compression strut is calculated from Eq. (3). Ref. 7 recommends an effective average bond stress of $2.0\sqrt{f_c'}$ MPa ($24\sqrt{f_c'}$ psi), which is slightly less than the value calculated from these test results.

4. The amount of column bar force to be carried by the strut-and-tie mechanism, ΔT_2 is then determined as:

$$\Delta T_2 = T_1 + C_{s1} - \Delta T_1 \qquad (4)$$

where T_1 and C_{s1} are the tension and compression forces in the outer layer of bars at the top and bottom of the joint boundary, as shown in Fig. 15.

5. The required amount of transverse joint reinforcement is then found from:

$$A_{jh} = \frac{\Delta T_2}{f_{yh}\tan\theta} \qquad (5)$$

where θ is the angle subtended by the horizontal axis and the line from the center of compression of the beam and column compression resultants to the intersection of the extreme column bar at the joint midheight, as shown in Fig. 15.

6. It is assumed that the forces in the interior column bars can be transferred by bond within the major diagonal strut. This was clearly not a problem with the two units tested in this series, and it can be argued that the additional width of the joint compression field resulting from hoop action will always result in a satisfactory performance of the inner layer, if Eq. (5) is satisfied for the outer layers.

CONCLUSIONS

Preliminary tests on two large-scale ungrouted prestressed, precast concrete beam-to-column subassemblages representing an interior and exterior joint, respectively, lead to the following conclusions:

1. The interior and exterior joints attained interstory drifts of 2.8 and 4 percent, respectively, without significant strength degradation. This exceeded the design level of drift by 40 and 100 percent, respectively.

2. Cracks were well distributed over the joint and there was no joint failure even though only nominal joint shear steel was provided. For the interior joint, the stirrup strain exceeded the yield strain and it is felt that slightly more conservative design requirements could be appropriate. A design approach to determine required transverse reinforcement to prevent bond failure of the column bars within the joint was developed based on a rational analysis of the joint behavior.

3. Very little energy was absorbed in the hysteresis loops during cycles to the same displacement level. The stiffness decreased with cycles to larger displacements as a consequence of inelastic compression stresses developing at the top and bottom of the beam plastic hinges "softening" the response.
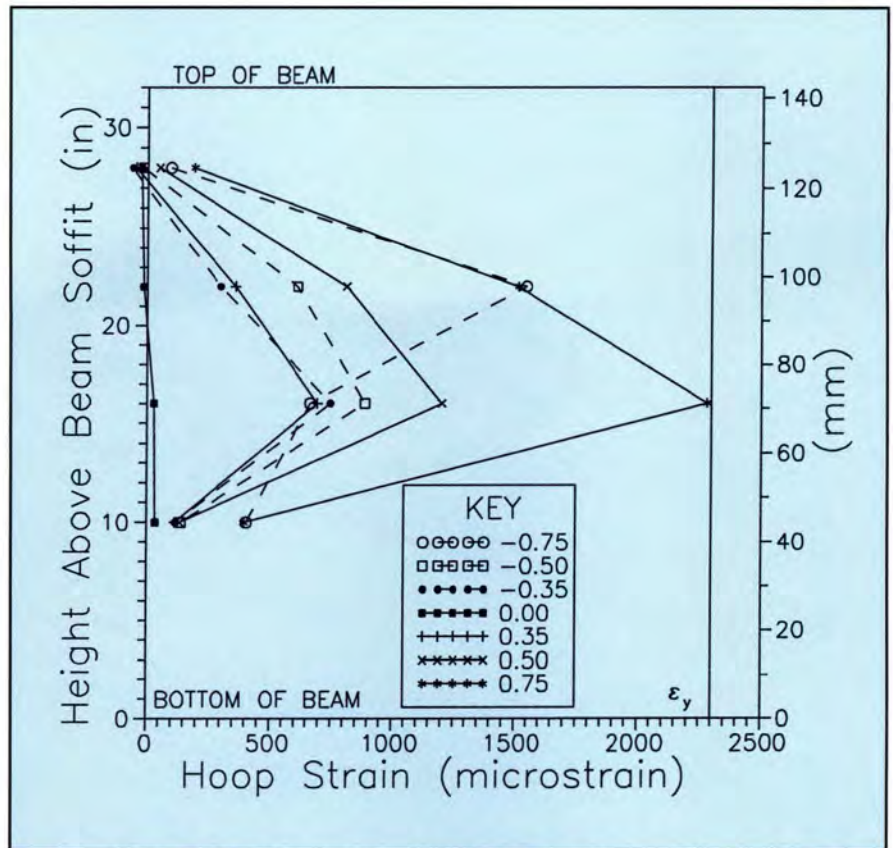

Fig. 13a. Joint shear strains at different drifts. Interior subassemblage up to 0.75 percent drift level.
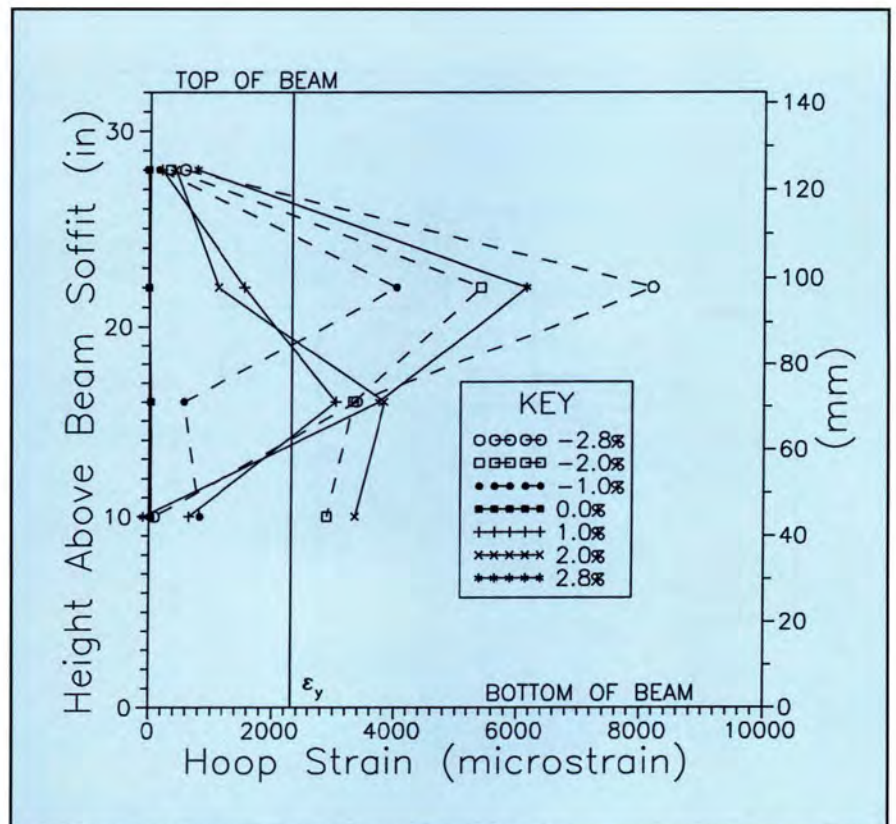

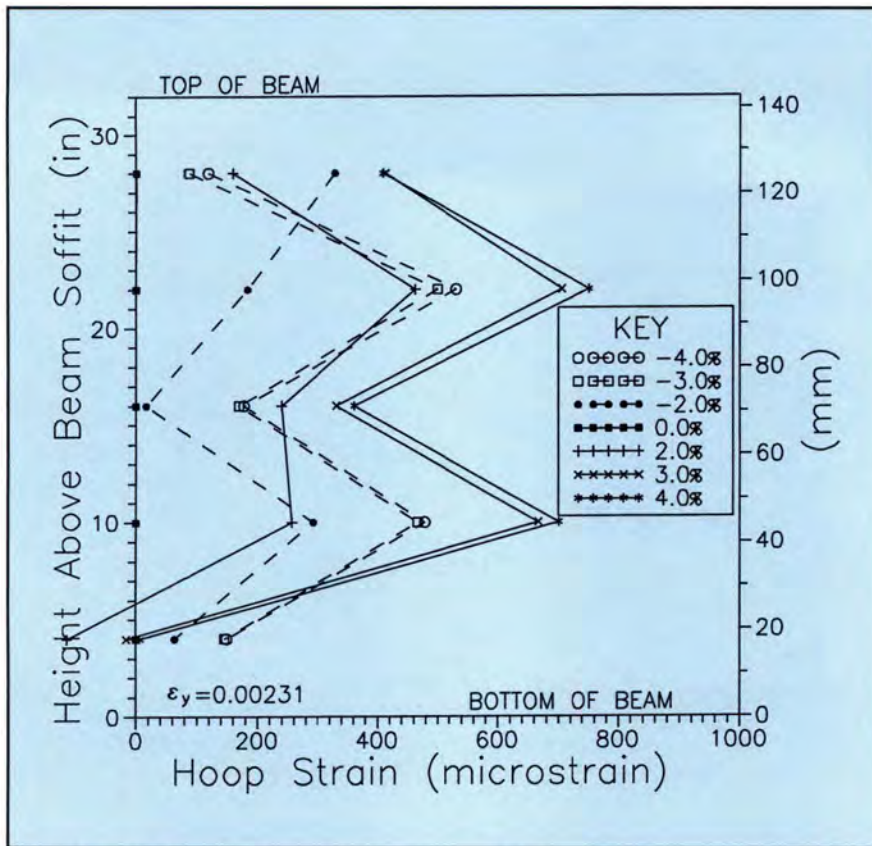Fig. 13b. Joint shear strains at different drifts. Interior subassemblage up to 1.00 percent drift level.

Fig. 13c. Joint shear strains at different drifts. Exterior subassemblage at high drift levels.
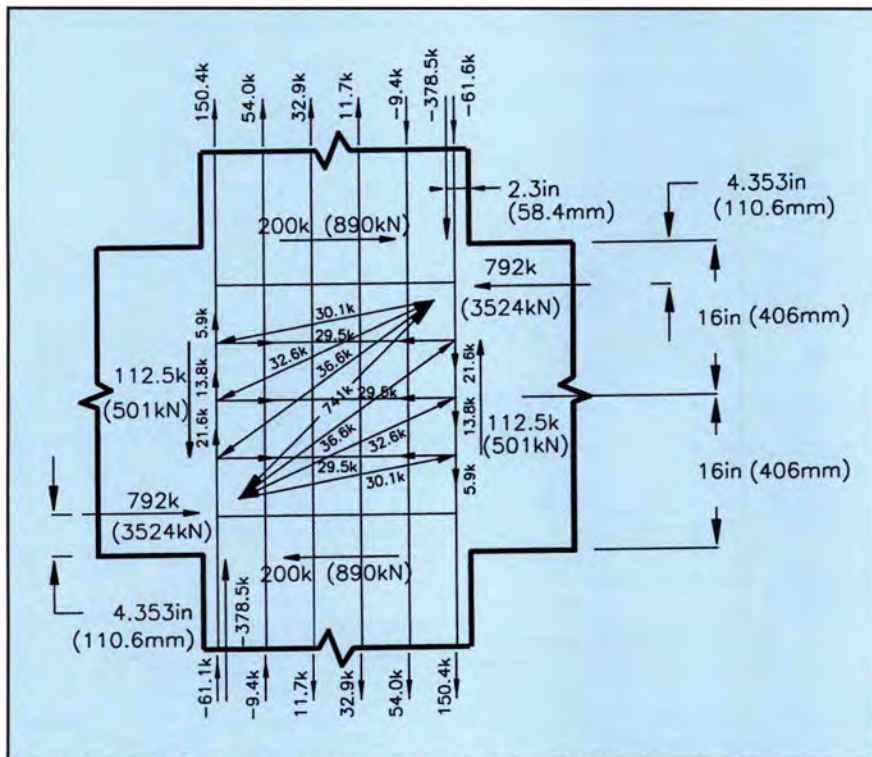

Fig. 14a. Possible strut-and-tie models of joint region at maximum response; interior subassemblage.

4. Damage to the specimens after completion of testing was small, indicating that very little repair would be required to reinstate this type of joint after a major earthquake. It is felt that the initial stiffness could readily be regained by epoxy grouting the cracks.

5. The maximum residual displacements were approximately 2.2 percent of the maximum drift, indicating that after an earthquake the structure is likely to have very low residual displacements and will probably return to near its original displacement.

6. A method to approximate the hysteretic behavior of subassemblages was developed in order that the maximum likely displacements of these structures can be evaluated using inelastic time history analysis.

7. Further research is needed to characterize the hysteretic response, to optimize joint design, to determine the extent that special confinement reinforcement is needed in the plastic hinge region, and to investigate the shear design of the beams. Current tests in a continuation of the research should provide much of this information.

8. The structural response was very satisfactory, despite the very low levels of reinforcement provided in the beams, columns, and joints. Based on these results, the concept of ungrouted prestressed, precast frames warrants a more detailed research investigation. In comparison with equivalent monolithic reinforced concrete construction, the test units absorbed less energy but suffered much less damage and sustained lower residual drift. Because of increased initial stiffness compared with a reinforced concrete unit of similar dimensions and strength, peak response displacements of the two systems are likely to be similar.

DESIGN RECOMMENDATIONS

The test results support the design of precast concrete frames with unbonded tendons for seismic regions. Based on the results, the following preliminary recommendations are made:
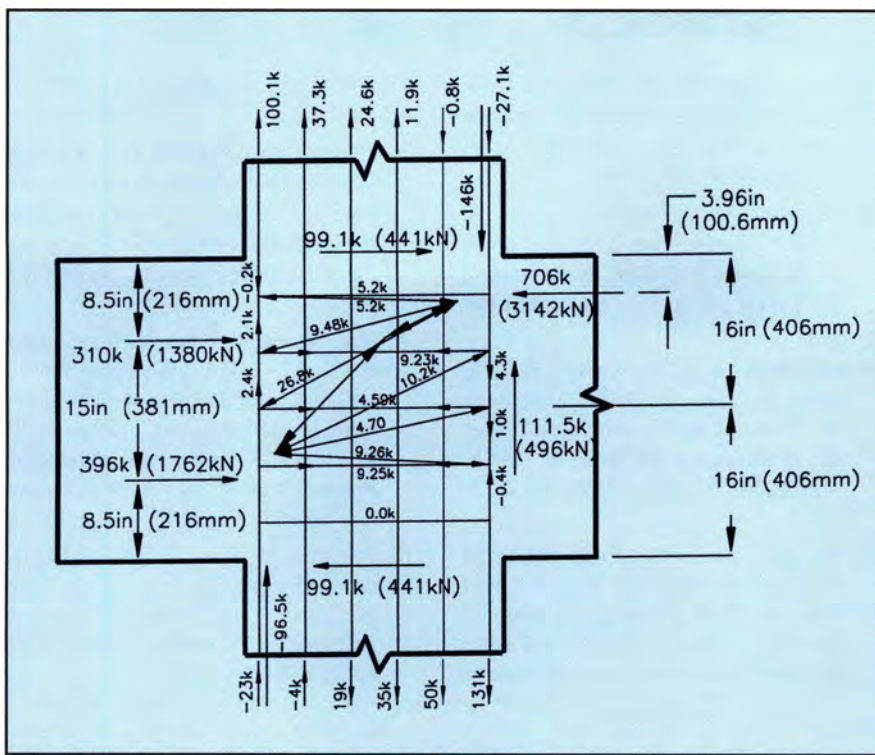
Fig. 14b. Possible strut-and-tie models of joint region at maximum response; exterior subassemblage.
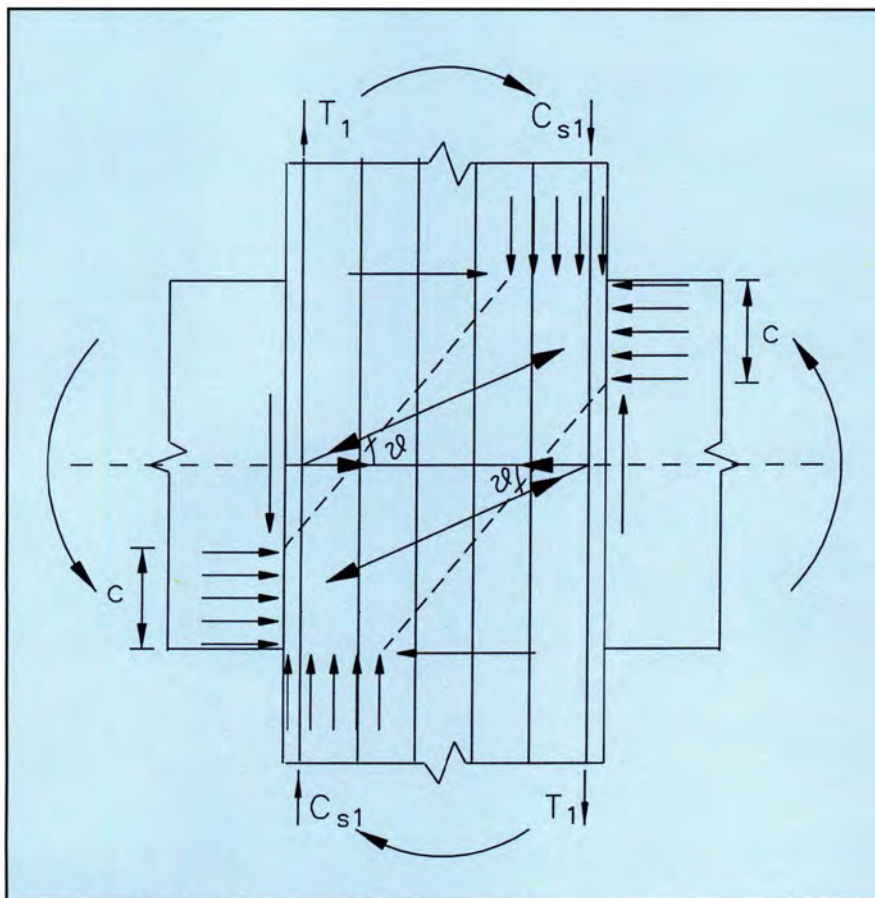

Fig. 15. Joint strut-and-tie model for the design of transverse reinforcing steel.

1. The flexural strength of the unbonded precast beams can be based on the tendon force at the limit of proportionality strain, using normal flexural strength theory.

2. A design drift limit of 2 percent can be conservatively adopted.

3. Joint reinforcement may be reduced below that required by current seismic codes. A design method outlined in the paper agreed well with observed performance.

4. It is clear that the hysteretic characteristics are different from those envisaged for ductile systems in the Uniform Building Code seismic design approach, which may thus be inappropriate for precast frames with unbonded tendons. An alternative approach currently under consideration, which shows considerable promise, is to use a displacement-based rather than a force-based procedure.[10] In this approach, the structure is designed to achieve the specified drift limit using an elastic displacement response spectrum and elastic characteristics based on an equivalent secant structural stiffness and damping at the design drift limit, rather than on the initial elastic characteristics. Based on the test results reported in this paper, it appears that equivalent viscous damping of 10 percent would be appropriate for this approach.

ACKNOWLEDGMENT

REFERENCES

1. Priestley, M. J. N., and Tao, J., "Seismic Response of Precast Prestressed Concrete Frames With Partially Debonded Tendons," PCI JOURNAL, V. 38, No. 1, January-February 1993, pp. 58-69.

2. MacRae, G. A., and Priestley, M. J. N., "Precast Post-Tensioned Ungrouted Concrete Beam-Column Subassemblage Tests," Structural Systems Research Report No. SSRP 94/10, University of California at San Diego, La Jolla, CA, March 1988, 124 pp.

3. Mander, J. B., Priestley, M. J. N., and Park, R., "Theoretical Stress-Strain Model for Confined Concrete," *Journal of the Structural Division*, ASCE, V. 114, No. 8, August 1988, pp. 1804-1826.

4. ACI Committee 318, "Building Code Requirements for Reinforced Concrete (ACI 318-89)," American Concrete Institute, Detroit, MI, 1989.

5. Popovics, S., "A Numerical Approach to the Complete Stress-Strain Curves for Concrete," *Cement and Concrete Research*, V. 3, No. 5, September 1973, pp. 583-599.

6. Priestley, M. J. N., Verma, R., and Xiao, Y., "Seismic Shear Strength of Reinforced Concrete Columns," *Journal of Structural Engineering*, ASCE, V. 120, No. 8, August 1994, pp. 2310-2329.

7. Priestley, M. J. N., "Assessment and Design of Joints for Single-Level Bridges With Circular Columns," Structural Systems Research Report No. 93/02, University of California at San Diego, La Jolla, CA, February 1993, 62 pp.

8. "Report on the Third U.S. PRESSS Coordinating Meeting," PRESSS Report No. 92/02, M. J. N. Priestley (Editor), University of California at San Diego, La Jolla, CA, August 6-7, 1992.

9. Eligehausen, R., Popov, E. P., and Bertero, V. V., "Local Bond Stress-Slip Relationships of Deformed Bars Under Generalized Excitation," Report UCB/EERC-83/23, Earthquake Engineering Research Center, University of California, Berkeley, CA, 1983, 178 pp.

10. Priestley, M. J. N., "Myths and Fallacies in Earthquake Engineering," Proceedings, Thomas Paulay Symposium, ACI Special Publication SP157, 1995, pp. 231-254.

APPENDIX — NOTATION

A_{jh} = transverse joint reinforcement area

c = compression zone depth at beam flexural strength

C_1 = compression force in column compression zone above joint

C_2 = compression force in column compression zone below joint

C_{s1} = compression force in outer layer bars

D = turn diameter of confining spiral

E_c = elastic modulus of concrete

f_c' = concrete cylinder compression stress

f_{cc}' = compressive stress of confined concrete

f_{pu} = tendon nominal tension strength

f_u = ultimate stress of reinforcing bars

f_y = yield stress of reinforcing bars

f_{yh} = transverse joint reinforcement yield stress

H = lateral force

K = parameter used for bond stress calculations

M_{Bl} = beam moment on left of joint

M_{Br} = beam moment on right of joint

M_{Cl} = column moment below joint

M_{Cu} = column moment above joint

M_{lp} = beam flexural strength

M_n = column ideal flexural strength

P = axial force

T_{c1} = tension force in column longitudinal reinforcing bars above joint

T_{c2} = tension force in column longitudinal reinforcing bars below joint

T_1 = tension force in outer layer bars or tension force in upper tendon

T_2 = tension force in lower tendon

u_u = ultimate bond stress

V_{Bl} = beam shear on left of joint

V_{Br} = beam shear on right of joint

V_c = contribution of concrete to shear strength

V_{Cl} = column shear joint

V_{Cu} = column shear above joint

V_j = joint shear force

V_{jh} = joint horizontal shear force

V_{jv} = joint vertical shear force

V_n = shear strength

V_p = contribution of axial force to shear strength

V_s = contribution of steel to shear strength

α = parameter for unloading of hysteresis loop

δ_1 = displacement

δ_2 = displacement

δ_3 = displacement

δ_4 = displacement

Δ = displacement

ΔT = bond force transferred in outer layer of compression bars in compression zone

ΔT_1 = force transferred by bond within compression zone

ΔT_2 = bar force carried by strut and tie mechanism

ε_{cu} = ultimate compression strain of confined concrete

ε_y = reinforcing bar yield strain

θ = angle

θ_m = maximum drift ratio

θ_r = residual drift ratio

ρ_s = volumetric ratio of confining steel

Σ_o = surface area per unit length of reinforcing bar

ϕ_s = strength reduction factor